Journal of Catalysis 286 (2012) 273–278

Contents lists available at SciVerse ScienceDirect

Journal of Catalysis

journal homepage: www.elsevier.com/locate/jcat

Effect of phase structures of $TiO_{2-x}N_y$ on the photocatalytic activity of $CaAl_2O_4$:(Eu, Nd)-coupled $TiO_{2-x}N_y$

Huihui Li [a,b,*], Shu Yin [a], Yuhua Wang [b], Tsugio Sato [a]

[a] Institute of Multidisciplinary Research for Advanced Materials, Tohoku University, 2-1-1, Katahira, Aoba-ku, Sendai 980-8577, Japan
[b] Lanzhou University, 222, Tianshuinan Road, Lanzhou 730000, PR China

ARTICLE INFO

Article history:
Received 18 August 2011
Revised 24 October 2011
Accepted 21 November 2011
Available online 23 December 2011

Keywords:
Crystalline phase
TiO_2-based composite photocatalyst
Persistent catalytic activity

ABSTRACT

Nitrogen-doped titanium oxide ($TiO_{2-x}N_y$) nanocrystalline with different phase of anatase, rutile or brookite was coupled with $CaAl_2O_4$:(Eu, Nd) particles by planetary ball milling treatment. The effect of phase structures on the persistent photocatalytic activity of a $CaAl_2O_4$:(Eu, Nd)/$TiO_{2-x}N_y$ composite was evaluated for the oxidative destruction of NO. The persistent catalytic degradation of NO by $TiO_{2-x}N_y$ was realized in the presence of $CaAl_2O_4$:(Eu, Nd), which shows a long afterglow luminescence. The persistent photocatalytic property of composites changed depending on the crystalline phase of $TiO_{2-x}N_y$, i.e., the persistent photocatalytic property of $CaAl_2O_4$:(Eu, Nd) combined with brookite type $TiO_{2-x}N_y$ was superior to those of anatase or rutile phase $TiO_{2-x}N_y$.

1. Introduction

TiO_2 photocatalysis has attracted increasing attention due to its biological and chemical inertness, strong photooxidation power, cost-effectiveness and long-term stability against photo and chemical corrosion [1–5]. However, a vital problem, that is, low utilization efficiency of sunlight due to its large band gap energy of ca. 3 eV, which covers less than 5% of the solar spectrum, hampers its widespread practical applications [6]. Therefore, various modifications have been devoted to TiO_2 to extend the absorption edge into the visible light in order to enhance the visible light responsive photocatalytic activity [7–12]. One of them is doping TiO_2 with nitrogen because the band gap of titania could be narrowed by doping with nitrogen ion since the valence band of N2p band locates above O2p band [13].

A novel approach to improve the photocatalytic efficiency of TiO_2, which attempts to prepare supported TiO_2 catalysts using long afterglow phosphor as material support, has been made; in this case, the aim was to associate a fluorescence-emitting support to TiO_2 to continue the photocatalytic reaction after turning off the light. The aluminate long afterglow phosphor ($CaAl_2O_4$:(Eu, Nd)) has characteristics of high luminescent brightness around 440 nm of wavelength, long afterglow time, good chemical stability and low toxicity [14,15]. These advantages have brought $CaAl_2O_4$:(Eu, Nd) phosphor into the most popular commercial products. The luminescent brightness around 440 nm can excite the visible light responsive nitrogen-doped titania ($TiO_{2-x}N_y$), while it is invalid to undoped TiO_2. Therefore, $TiO_{2-x}N_y$ photocatalyst was expected to possess a novel photocatalytic property after coupling with $CaAl_2O_4$:(Eu, Nd) [16,17].

Recently, a direct evidence for such persistent photocatalytic reaction has been reported for deNO_x system, by the coupling of the long afterglow phosphor $CaAl_2O_4$:(Eu, Nd) with $TiO_{2-x}N_y$, which was produced by a hydrothermal reaction [18]. However, the effect of the TiO_2 phase structure on the photocatalytic properties of $CaAl_2O_4$:(Eu, Nd)/$TiO_{2-x}N_y$ composites has not been systematically studied yet.

In this work, $TiO_{2-x}N_y$ samples with three different phase structures, such as anatase, rutile and brookite, were coupled with similar contents of $CaAl_2O_4$:(Eu, Nd) by a mild planetary ball milling, and the photocatalytic activities of the composites for the oxidative destruction of NO were investigated.

2. Experimental

2.1. Preparation of photocatalysts

$CaAl_2O_4$:(Eu, Nd) powders (Nemoto Co. Ltd.) with particle size of 13.9 μm (D_{50}) and other chemicals (Kanto Chem. Co. Inc. Japan) were used as received without further purification. $TiO_{2-x}N_y$ nanoparticles with brookite, anatase and rutile phases were synthesized by the solvothermal reactions according to the previous papers [16], using $TiCl_3$ as a titanium source, HMT (hexamethylenetetramine) as a nitrogen source, and distilled water, methanol and

* Corresponding author at: Institute of Multidisciplinary Research for Advanced Materials, Tohoku University, 2-1-1, Katahira, Aoba-ku, Sendai 980-8577, Japan. Fax: +81 22 217 5598.
E-mail address: lihuihui@mail.tagen.tohoku.ac.jp (H. Li).

0021-9517/$ - see front matter © 2011 Elsevier Inc. All rights reserved.
doi:10.1016/j.jcat.2011.11.013

ethanol as the reaction solvents at pH 7 or 9 and 190 °C for 2 h [16]. $TiO_{2-x}N_y$ nanoparticles with different phase were then mixed with $CaAl_2O_4$:(Eu, Nd) microparticles followed by a soft planetary ball milling with 200 rpm for 20 min, where the mass ratio of $CaAl_2O_4$:(Eu, Nd)/$TiO_{2-x}N_y$ was adjusted to 3/2. For comparison, undoped titania (Degussa P25) was also coupled with $CaAl_2O_4$:(Eu, Nd) by the completely same manner. The UV–vis diffuse reflectance spectra were obtained using a UV–vis spectrophotometer (Shimadazu, UV-2450). The photoluminescence spectra and intensity were measured by a spectrofluorophotometer (Shimadzu RF-5300P). The low-level chemiluminescence intensity of singlet oxygen ($^1O_2$) was measured using a multiluminescence spectrometer (MLA-GOLDS; Tohoku Electric Ind., Japan) at 20 °C in the air. After placing approximately 1.2 g of the sample in a stainless steel sample chamber (50 mm in diameter), blue light-emitting diode (LED) light (wavelength 470 nm) was irradiated for 5 min. After that, the chemiluminescence intensity corresponded to the singlet oxygen ($^1O_2$) at a wavelength of 643 nm was measured by subtracting the luminous intensity of $\lambda < 640$ nm from that of $\lambda < 620$ nm using two filters, $\lambda < 640$ nm and $\lambda < 620$ nm.

2.2. Photocatalytic degradation characterization

The photocatalytic activity for NO destruction was determined by measuring the concentration of NO gas at the outlet of the reactor (373 cm^3 of internal volume) duringLanzhou University, PR China the photo-irradiation of a constantly flowing 1 ppm NO/50 vol% air-mixed (balance N_2) gas (200 cm^3 min^{-1}); 0.16 g of $CaAl_2O_4$:(Eu, Nd)/$TiO_{2-x}N_y$, $TiO_{2-x}N_y$ or $CaAl_2O_4$:(Eu, Nd)/P25 powders was placed on a glass holder plate with a hollow of 40 × 30 × 0.5 mm and set in the bottom center of the reactor. A solar simulator (HAL-302, Asahi Spectra Co. Ltd, Japan) with a compact xenon lamp was used as a light source, where the intensity of irradiation light was adjusted as 69.7 W/m^2. Before light irradiation, the NO gas was continuously flowed through the reactor for 10 min to achieve diffusion and adsorption balance. Then, keeping light source irradiation for 30 min to realize the steady status of the photocatalytic degradation of NO and make long afterglow phosphor $CaAl_2O_4$:(Eu, Nd) absorbs enough exciting energy. After that, the light was switched off, while the NO gas was flowed further for 3 h. In order to investigate the visible light response of nitrogen-doped TiO_2 and P25, photocatalytic activities of all samples were also tested in the same measuring system but under the LED light irradiation. The light wavelength was controlled by selecting two types of monochromatic LED lamps (SP-E27, 2.5 W; OptiLED) [19]. One is the blue light LED with the wavelength of 445 nm, and another one is the UV light LED with the wavelength of 390 nm. Photocatalytic reactions were carried out by irradiating these two LED lights at the same light irradiation intensity of 2 W/m^2 on the same area by controlling the irradiation distance.

3. Results and discussion

3.1. Preparation of different crystalline phases of titania

Fig. 1 shows the X-ray diffraction (XRD) profiles of the $TiO_{2-x}N_y$ samples produced by solvothermal reactions under various conditions. The sample prepared in methanol at pH 9 and 190 °C consisted of single phase of anatase. The sample prepared in ethanol at pH 9 and 190 °C consisted of single-phase rutile, showing the broad XRD peak at $2\theta = 27.42°$ corresponding to (1 1 0) of rutile phase. The sample prepared in water at pH 7 and 190 °C showed the clear XRD peak at $2\theta = 30.81°$ corresponding to (1 2 1) of the brookite phase, and all peaks could be identified as the brookite phase. Therefore, it was confirmed that three different phases of

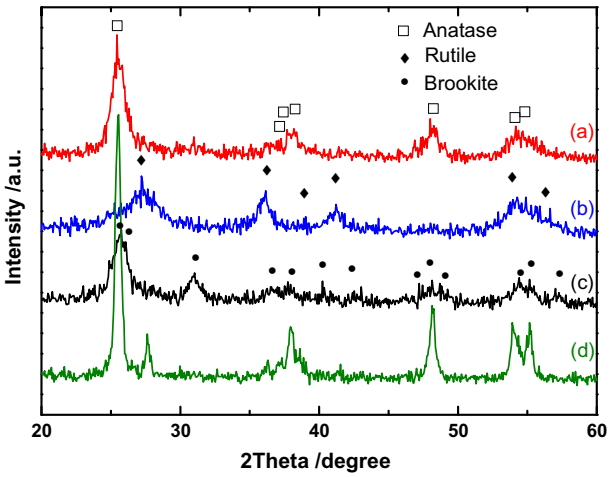

Fig. 1. XRD patterns of the nitrogen-doped TiO_2 synthesized at 190 °C for 1 h in (a) methanol at pH 9, (b) ethanol at pH 9, (c) distilled water at pH 7 and (d) P25.

$TiO_{2-x}N_y$ powders could be prepared as single phase by controlling the solvothermal reaction conditions. As reported, P25 consisted of the mixed phase of anatase and rutile. The average crystalline sizes and BET surface areas (BET from Brunauer, Emmett, Teller) of TiO_2 samples are listed in Table 1. It can be seen that these TiO_2 samples possess similar average crystallite sizes less than 10 nm, while anatase phase $TiO_{2-x}N_y$ sample shows the largest BET surface area of 254.4 m^2/g.

3.2. Morphology of the samples

Fig. 2 shows the transmission electron microscopy (TEM) images of the anatase, rutile and brookite phases of $TiO_{2-x}N_y$ powders prepared by the solvothermal reactions, together with that of P25. P25 consisted of large spherical particles of about 30–50 nm (Fig. 2d), while $TiO_{2-x}N_y$ prepared by the solvothermal method consisted of much smaller crystals (Fig. 2a–c). The results agreed well with the BET-specific surface areas summarized in the Table 1, i.e., the specific surface area of as-prepared nitrogen-doped TiO_2 was much larger than that of P25.

Fig. 2e and f shows the TEM images of $CaAl_2O_4$:(Eu, Nd)/$TiO_{2-x}N_y$ composite and uncoupled $CaAl_2O_4$:(Eu, Nd), respectively. It is obvious that $CaAl_2O_4$:(Eu, Nd) phosphor sample consisted of micrometer size of large particle with a smooth surface (Fig. 2f), while the $CaAl_2O_4$:(Eu, Nd)/$TiO_{2-x}N_y$ composite showed nanoparticles of $TiO_{2-x}N_y$ deposited on the surface of $CaAl_2O_4$:(Eu, Nd).

3.3. UV–vis diffuse reflectance spectra

Fig. 3A shows the diffuse reflectance spectra of undoped and nitrogen-doped titania and the emission spectra of $CaAl_2O_4$:(Eu, Nd) and $CaAl_2O_4$:(Eu, Nd)/$TiO_{2-x}N_y$ composites. $CaAl_2O_4$:(Eu, Nd) emitted blue luminescent light with a peak of 440 nm in wavelength by UV light irradiation (325 nm). Although undoped titania

Table 1
Physical properties of nitrogen-doped titania.

Sample	BET-specific surface area (m^2 g^{-1})	Crystallite size of TiO_2 (nm)
Anatase phase $TiO_{2-x}N_y$	254.4	9
Rutile phase $TiO_{2-x}N_y$	218.2	6.3
Brookite phase $TiO_{2-x}N_y$	149.5	8.5
Degussa P25	47.3	18.6

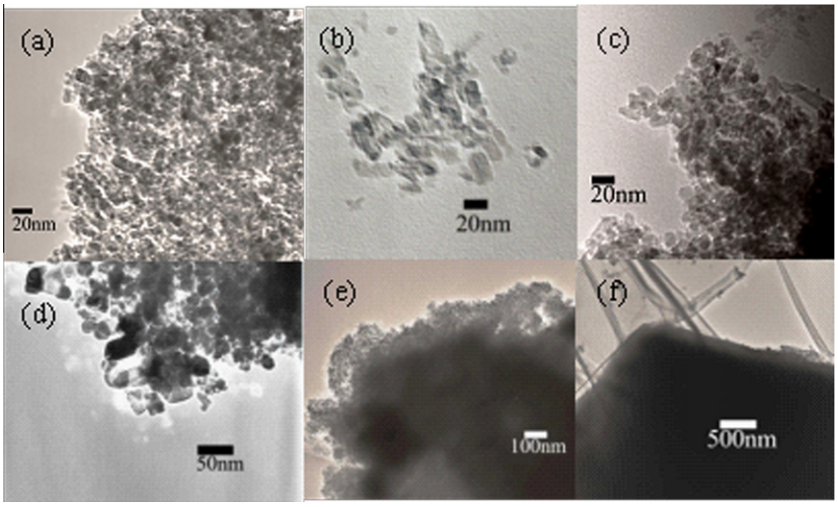

Fig. 2. TEM images of $TiO_{2-x}N_y$ of (a) anatase, (b) rutile, (c) brookite phase, (d) P25 TiO_2, (e) fringe area of $CaAl_2O_4$:(Eu, Nd)/brookite $TiO_{2-x}N_y$ composite and (f) uncoupled $CaAl_2O_4$:(Eu, Nd).

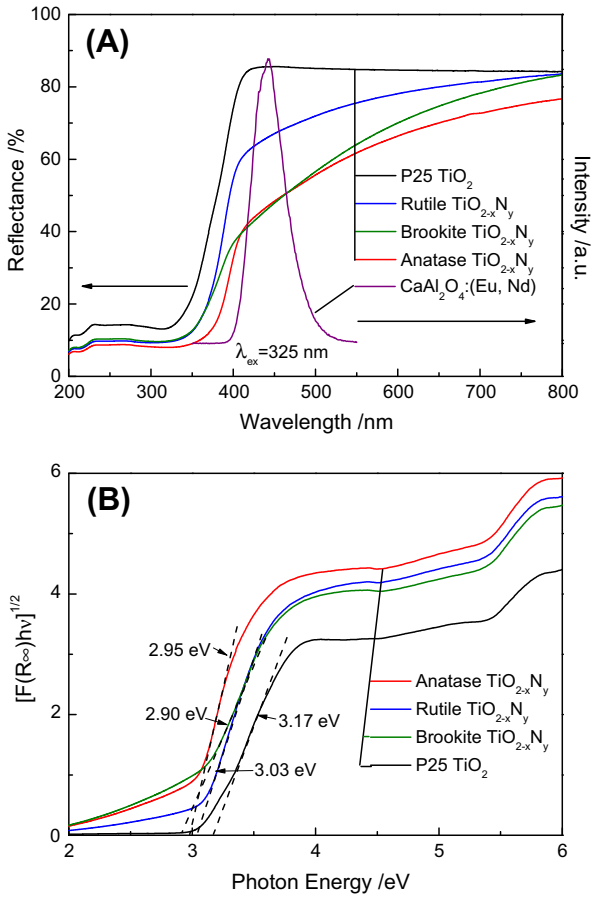

Fig. 3. (A) Overlap of the diffuse reflectance spectra and emission spectra of uncoupled $CaAl_2O_4$:(Eu, Nd) and $CaAl_2O_4$:(Eu, Nd)/TiO_2−*x*Ny composite and (B) absorption edge energies are determined by the intercept of a linear fit to the absorption edge. $[F(R_\infty)h\nu]$ represents the Kubelka–Munk function multiplied by the photon energy.

absorbed only UV light of the wavelength less than 400 nm, nitrogen-doped titania showed absorption of visible light up to 700 nm, showing a nice overlap between the diffuse reflectance spectrum of $TiO_{2-x}N_y$ and the emission spectrum of $CaAl_2O_4$:(Eu, Nd). These results implied the potential possibility of $CaAl_2O_4$:(Eu, Nd)/$TiO_{2-x}N_y$ composite as the luminescent assisted photocatalyst, which can use the long after glow from the phosphor as the light source of the photocatalyst. As shown in Fig. 3B, the position of the absorption edge also allows comparisons between the TiO_2 samples with different phase reported here. The edge energy value of 2.90 eV of brookite phase $TiO_{2-x}N_y$ indicates the higher property to be induced by the fluorescence with the wavelength of 440 nm from $CaAl_2O_4$:(Eu, Nd). Our previous research proved that photocatalysis on $TiO_{2-x}N_y$ could take place under LED lamp irradiation, and only low-intensity LED light as 2.0 W/m^2 with long wavelength of 627 nm [19,20] was used. This result also strongly implied the potential application of the composite as luminescent assisted photocatalyst material.

3.4. Luminescent decay profiles

Phosphorescence from $CaAl_2O_4$:(Eu, Nd) crystals is considered due to the 5d-4f transition of the Eu^{2+} ions in the crystals. The long afterglow from $CaAl_2O_4$:(Eu, Nd) is proposed based on the hole trapping by the Nd^{3+} ions added as an auxiliary activator. The holes generated by the excitation of Eu^{2+} are trapped by co-doped Nd^{3+} ions and/or native defects. Holes trapped at Nd and/or defects are released slowly and then recombine with electrons from the Eu^{2+} ions. This process is thought to be the origin of the long persistent phosphorescence from $CaAl_2O_4$:(Eu, Nd) [21,22]. In order to investigate the photoelectric properties of $CaAl_2O_4$:(Eu, Nd)/$TiO_{2-x}N_y$, the PL spectra were detected for the different composite samples after exiting by UV light irradiation as shown in Fig. SI-3. The PL intensity greatly decreased by loading with $TiO_{2-x}N_y$ and P25 on the surface of the $CaAl_2O_4$:(Eu, Nd). From the figure, the peak wavelengths of the phosphorescence spectra did not change with the loading of $TiO_{2-x}N_y$ or P25. It implies that the crystal field of $CaAl_2O_4$:(Eu, Nd), which affects the 5d electron states of Eu^{2+} ions, is not changed so much for the present composites. The intensity of the emission from the $CaAl_2O_4$:(Eu, Nd) decreased by coupling with P25 and $TiO_{2-x}N_y$. This may be due to the absorption of both UV light to excite the $CaAl_2O_4$:(Eu, Nd) phosphor and luminescence light by coupled P25 and $TiO_{2-x}N_y$. It can also be seen that the luminescence intensity of the $CaAl_2O_4$:(Eu, Nd)/$TiO_{2-x}N_y$ particles is much lower than that of the $CaAl_2O_4$:(Eu, Nd)/P25. This suggests that $TiO_{2-x}N_y$ particles deposited on the surface could absorb the luminescence light more effectively than P25.

Fig. 4 shows the decay profiles of the various samples. The profile varied depending on the coupled materials. The decay curves could be fitted to the triple exponential curve shown by Eq. (1) [23],

$$I = \alpha \exp(-t/\tau_1) + \beta \exp(-t/\tau_2) + \gamma \exp(-t/\tau_3) \quad (1)$$

where I is phosphorescence intensity, I_0 is the starting phosphorescence intensity, α, β and γ are constants, t is time, and τ_1, τ_2 and τ_3 are emission lifetimes. The emission lifetimes calculated based on Eq. (1) are summarized in Table 2. From Table 2, it is evident that the decay of phosphorescence includes several decay components with different emission lifetimes. The emission lifetimes of the $CaAl_2O_4$:(Eu, Nd) crystals did not change so much by coupling with both P25 and $TiO_{2-x}N_y$. This indicates that the quenching of luminescence by the heterogeneous electron transfer from $CaAl_2O_4$:(Eu, Nd) to coupled P25 and $TiO_{2-x}N_y$ did not proceed significantly.

Fig. 5 shows the chemiluminescence emission spectra of $^1O_2$ generated at 20 °C in the air by blue light irradiation with a wavelength of 470 nm. $TiO_{2-x}N_y$ with anatase phase and rutile phase showed very weak chemiluminescence. In contrast, the brookite phase $TiO_{2-x}N_y$ showed much higher chemiluminescence intensity, indicating that brookite phase $TiO_{2-x}N_y$ generated much more $^1O_2$. Since it is well known that $^1O_2$ possesses strong oxidation power and plays an important role to cause photocatalytic oxidation reactions, $CaAl_2O_4$:(Eu, Nd)/brookite $TiO_{2-x}N_y$ is expected to show high photocatalytic activity.

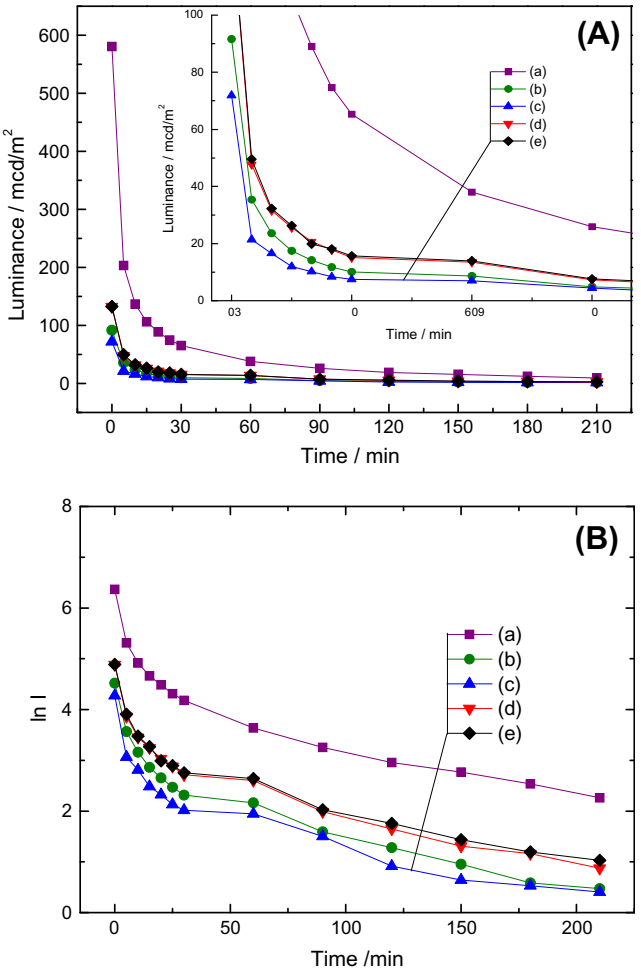

Fig. 4. Decay curves of (A) emission intensity (I) and (B) ln I of (a) uncoupled $CaAl_2O_4$:(Eu, Nd) and $CaAl_2O_4$:(Eu, Nd)/$TiO_{2-x}N_y$ composite consisted of 40 wt.% of (b) anatase phase $TiO_{2-x}N_y$, (c) rutile phase $TiO_{2-x}N_y$, (d) brookite phase $TiO_{2-x}N_y$ and (e) P25 TiO_2 after mercury lamp ($\lambda > 290$ nm) irradiation for 30 min.

Table 2
Simulated results for the afterglow curves of samples.

Phosphor composition	τ_1 (min)	τ_2 (min)	τ_3 (min)
$CaAl_2O_4$:(Eu, Nd)	4.76	64.88	142.45
$CaAl_2O_4$:(Eu, Nd)/anatase $TiO_{2-x}N_y$	5.26	55.42	123.58
$CaAl_2O_4$:(Eu, Nd)/rutile $TiO_{2-x}N_y$	4.13	58.27	125.58
$CaAl_2O_4$:(Eu, Nd)/brookite $TiO_{2-x}N_y$	4.90	54.59	123.58
$CaAl_2O_4$:(Eu, Nd)/P25 TiO_2	4.90	54.59	123.58

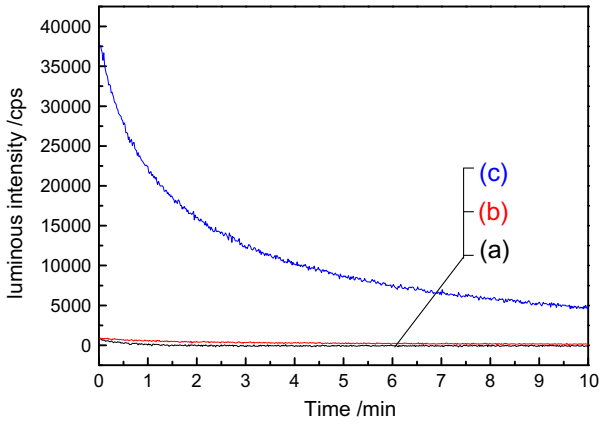

Fig. 5. Chemiluminescence spectra of as-prepared $TiO_{2-x}N_y$ particles with (a) anatase phase, (b) rutile phase and (c) brookite phase after blue light irradiation with a wavelength of 470 nm.

3.5. Photocatalytic degradation of NO gas

The photocatalytic activities of $CaAl_2O_4$:(Eu, Nd)/$TiO_{2-x}N_y$ with three different crystalline phases were evaluated for the oxidative destruction of NO. Table 3 shows the photocatalytic degradation of NO ($deNO_x$) ability of $TiO_{2-x}N_y$ powders with different crystalline phases under irradiation of blue (445 nm) and near-UV LED (390 nm) lamps. The wavelength of blue LED light is similar to the peak wavelength of the long afterglow by $CaAl_2O_4$:(Eu, Nd). For comparison, the standard titania photocatalyst (P25) and $CaAl_2O_4$:(Eu, Nd) phosphor were also characterized. Nearly 55–60% of NO could be destructed under irradiation of both LED lights in the presence of $TiO_{2-x}N_y$. It can be seen that although P25 showed similar photocatalytic activity to $TiO_{2-x}N_y$ under UV LED light irradiation, the activity greatly decreased under irradiation of blue LED light, due to its large band gap energy of ca. 3 eV, where the pho-

Table 3
$DeNO_x$ ability of the $TiO_{2-x}N_y$ samples under LED light irradiation (2.0 W/m^2) of 445 and 390 nm.

Photocatalyst	$DeNO_x$ ability under LED lamp irradiation (%)	
	Blue light (445 nm)	UV light (390 nm)
P25 TiO_2	13.2	56.2
Anatase $TiO_{2-x}N_y$	54.6	58.4
Rutile $TiO_{2-x}N_y$	55.8	60.9
Brookite $TiO_{2-x}N_y$	54.1	60.0
$CaAl_2O_4$:(Eu, Nd)	23.1	28.0
$CaAl_2O_4$:(Eu, Nd)/anatase $TiO_{2-x}N_y$	54.6	60.7
$CaAl_2O_4$:(Eu, Nd)/rutile $TiO_{2-x}N_y$	42.9	60.1
$CaAl_2O_4$:(Eu, Nd)/brookite $TiO_{2-x}N_y$	54.3	55.3

tocatalytic activity of $CaAl_2O_4$:(Eu, Nd) was much lower under irradiation of both lights.

Fig. 6 shows the photocatalytic NO destruction behaviors of $CaAl_2O_4$:(Eu, Nd)/$TiO_{2-x}N_y$ composites with anatase, rutile and brookite phase and those of $CaAl_2O_4$:(Eu, Nd)/P25 under solar light irradiation and after turning off the light. It was obvious that all the samples possessed excellent photocatalytic $deNO_x$ activity under solar light irradiation. Because a continuous reaction system was utilized in the present study [21,22], after turning off the light, usually it took about 10 min to return to the initial NO concentration. The degree of NO destruction by $CaAl_2O_4$:(Eu, Nd)/P25 immediately decreased after turning off the light; this result was similar to that of pure $TiO_{2-x}N_y$ shown in SI-4. In contrast, as expected, $CaAl_2O_4$:(Eu, Nd)/$TiO_{2-x}N_y$, especially the composite sample using brookite phase $TiO_{2-x}N_y$, retained the NO destruction ability for about 3 h. Since the decay profile of the NO destruction degree of $CaAl_2O_4$:(Eu, Nd)/brookite $TiO_{2-x}N_y$ was similar to the emission decay profile shown in Fig. 4, the emission by $CaAl_2O_4$:(Eu, Nd) seemed to be effectively used as a light source to excite $TiO_{2-x}N_y$ photocatalyst. In addition, the higher ability to generate $^1O_2$ of $CaAl_2O_4$:(Eu, Nd)/brookite phase $TiO_{2-x}N_y$ shown in Fig. 5 might play an important role to show higher NO destruction ability after turning off the light than $CaAl_2O_4$:(Eu, Nd)/anatase phase $TiO_{2-x}N_y$ and $CaAl_2O_4$:(Eu, Nd)/rutile phase $TiO_{2-x}N_y$.

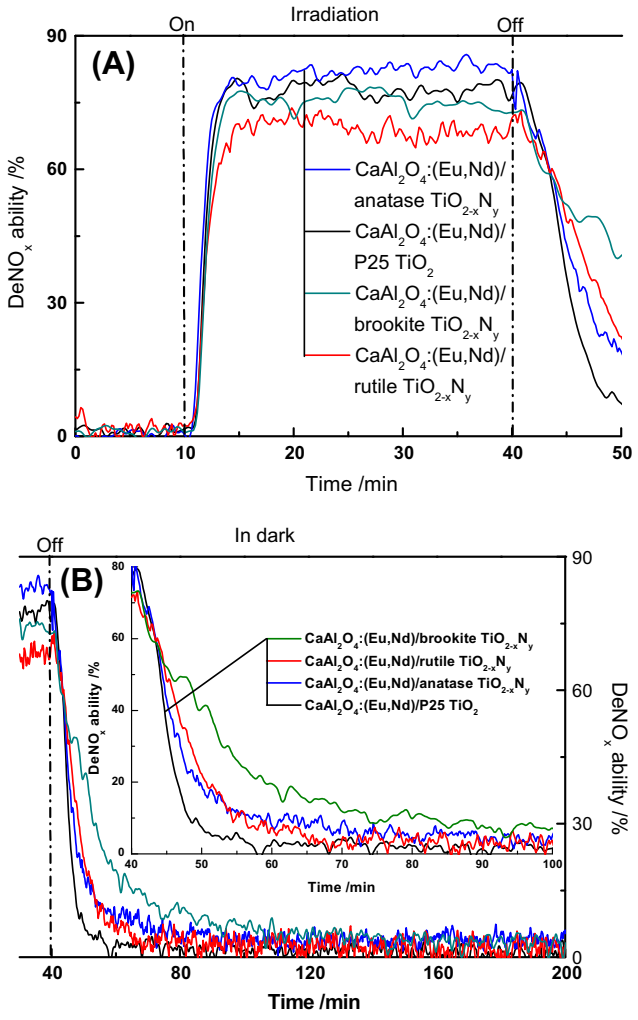

Fig. 6. $DeNO_x$ ability of the composites consisted of 40 wt.% of $TiO_{2-x}N_y$ and P25 under (A) solar light irradiation of 69.7 W/m^2, followed by (B) turning off light. The inset shows the result in dark from 40 to 100 min.

Table 4 summarized the photocatalytic $deNO_x$ abilities and apparent quantum efficiencies (QE_a) of the $TiO_{2-x}N_y$ and $CaAl_2O_4$:(Eu, Nd)/40 wt.% $TiO_{2-x}N_y$ composites with three different crystalline phases under irradiation of blue LED lamp (445 nm), and after turning off the simulated solar light. QE_a was calculated according to Eq. (2) (LED lamp, 445 nm) and Eq. (3) (fluorescence, 440 nm), respectively [19,24].

$$QE_{a,445\text{nm}} = \frac{F_{NO}\alpha_\lambda}{P_1 S A_\lambda} \times 100\% \quad (2)$$

$$QE_{a,440\text{nm}} = \frac{F_{NO}\alpha_\lambda}{P_2 S} \times 100\% \quad (3)$$

where F_{NO} (μmol s^{-1}) is the flow quantity of NO molecules in the reaction gas, α_λ (%) the $deNO_x$ ability of the photocatalyst, P_1 (μmol m^{-2} s^{-1}) the light quantity of LED lamp with the wavelength of 445 nm irradiated to the sample, A_λ the absorption ability to light with the wavelength of 445 nm and P_2 (μmol m^{-2} s^{-1}) the absorbed fluorescence light amount that generated from $CaAl_2O_4$:(Eu, Nd); the decline amount of fluorescence intensity between composite and pure $CaAl_2O_4$:(Eu, Nd) is regarded as the absorbed fluorescence light amount since the fluoresce intensity did not vary with the content of $CaAl_2O_4$:(Eu, Nd) in 0.16 g of $CaAl_2O_4$:(Eu, Nd)/γ-Al_2O_3 composites (SI-1). S (m^2) is the irradiated area of the sample ($S = 1.28 \times 10^{-3}$ m^2). It is clear that $CaAl_2O_4$:(Eu, Nd)/$TiO_{2-x}N_y$ composite possessed much higher QE_a both under irradiation of blue LED light and after turning off the simulated solar light than that of P25, due to the higher ability of visible light absorption. It is also notable that the QE_a after turning off the simulated solar light was much higher than that under irradiation of blue LED light. This result indicated that the weak luminescent light from $CaAl_2O_4$:(Eu, Nd) could be utilized more effectively than that under irradiation of an excess amount of light.

Present results suggested that the combination of $CaAl_2O_4$:(Eu, Nd) and brookite phase $TiO_{2-x}N_y$ is a key point to realize the excellent persistent catalytic activity even after turning off the light. Its higher luminescence intensity after turning off the light, higher $^1O_2$ generation ability as well as high efficiency in utilizing luminescence from $CaAl_2O_4$:(Eu, Nd) long afterglow material would result in the higher persistent $deNO_x$ ability.

3.6. Reaction models

Under light excitation, the luminescence process of Eu^{2+} includes two parts: one is that the electrons at the excited state re-

Table 4
Photocatalytic $deNO_x$ abilities and apparent quantum efficiencies of the samples under irradiation of LED light of 445 nm and fluorescence light from $CaAl_2O_4$:(Eu, Nd) at 100 min after turning off artificial solar light.

Photocatalyst	$DeNO_x$ ability (%)		Quantum efficiency (%)	
	LED light 445 nm	Fluorescence 440 nm, 100 min	LED light 445 nm	Fluorescence 440 nm, 100 min
P25	13.2	–	0.14	–
$TiO_{2-x}N_y$ with anatase phase	54.6	–	0.16	–
$TiO_{2-x}N_y$ with rutile phase	55.8	–	0.26	–
$TiO_{2-x}N_y$ with brookite phase	54.1	–	0.16	–
$CaAl_2O_4$:(Eu, Nd)	23.1	0	0.31	0
$CaAl_2O_4$:(Eu, Nd)/P25	5.0	0	0.05	0
$CaAl_2O_4$:(Eu, Nd)/$TiO_{2-x}N_y$ with anatase phase	54.6	3.2	0.24	0.24
$CaAl_2O_4$:(Eu, Nd)/$TiO_{2-x}N_y$ with rutile phase	42.9	3.4	0.31	0.24
$CaAl_2O_4$:(Eu, Nd)/$TiO_{2-x}N_y$ with brookite phase	54.3	8.5	0.21	0.76

turn to the ground state, and the other one is that the electrons in the trap energy level release in the excitation state and then return to the ground state due to the thermal disturbance. The first part of luminescence does not exist after the excitation is stopped. The electrons captured and stored at the trap energy level will be excited to $4f^6 5d$ excitation state with the help of thermal disturbance, and then the electrons return $^8S_{7/2}$ ground state in succession, which leads to the characteristic luminescence of Eu^{2+}. The number of electrons stored in the trap energy level is high density, and its depth is proper to releasing electrons at room temperature. So the phosphor possesses high afterglow brightness and long afterglow time [22]. For $TiO_{2-x}N_y$, there is a second band gap, and the energy gap from the valence band to the conduction band is about 2.3 eV [16], which is lower than the emitted blue photon energy from the $CaAl_2O_4$:(Eu, Nd) long afterglow phosphor. As well known, semiconductors could be excited by the photons with an energy equivalent to or higher than the band gap energy, which causes the formation of photoelectrons and holes. According to the TEM images, $CaAl_2O_4$:(Eu, Nd) and $TiO_{2-x}N_y$ are contacted very well. This allows the effective absorption of luminescence light from $CaAl_2O_4$:(Eu, Nd) with $TiO_{2-x}N_y$. Then, the excited $TiO_{2-x}N_y$ triggers photocatalysis even after turning off the light. In addition, photogenerated holes and electrons in well-crystallized brookite $TiO_{2-x}N_y$ were more efficient to proceed the photocatalytic reaction. This gives rise to the subsequent photocatalysis using the luminescence emitted from $CaAl_2O_4$:(Eu, Nd) as a light source.

4. Conclusions

$TiO_{2-x}N_y$ powders with anatase, rutile and brookite phases were successfully synthesized by solvothermal synthesis by varying the concentration of HMT and/or various reaction solvent. The $CaAl_2O_4$:(Eu, Nd)/$TiO_{2-x}N_y$ composite catalysts consisted of the same mass contents of $CaAl_2O_4$:(Eu, Nd), but different crystalline phases of $TiO_{2-x}N_y$ were prepared by soft planetary ball milling treatment. The $CaAl_2O_4$:(Eu, Nd)/$TiO_{2-x}N_y$ with brookite phase composite showed higher persistent deNO_x ability than that consisted of anatase or rutile phase. This might be related to its high crystallinity (less crystal defects) and comparative small band gap value of brookite phase. The $CaAl_2O_4$:(Eu, Nd)/$TiO_{2-x}N_y$ with brookite phase composite provided enough luminescence intensity for the photocatalytic reaction for more than 3 h after turning off the irradiation light. A promising strategy of coupling long afterglow phosphor with visible light responsive photocatalyst that possessing a certain phase structure has been established.

Acknowledgments

This research was supported in part by the Management Expenses Grants for National Universities Corporations from the Ministry of Education, Culture, Sports, Science for Technology of Japan (MEXT), and by the Grant-in-Aid for Science Research (Nos. 20360293 and 22651022).

Appendix A. Supplementary material

Supplementary data associated with this article can be found, in the online version, at doi:10.1016/j.jcat.2011.11.013.

References

[1] L.M. Wang, N. Wang, L.H. Zhu, H.W. Yu, H.Q. Tang, J. Hazard. Mater. 52 (2008) 93.
[2] T. Tachikawa, M. Fujitsuka, T. Majima, J. Phys. Chem. C 111 (2007) 5259.
[3] B.M. Graetzel, Nature 353 (1991) 737.
[4] F. Zhang, J. Zhao, T. Shen, H. Hidaka, E. Pelizzetti, N. Serpone, Appl. Catal. B: Environ. 15 (1998) 147.
[5] L.X. Yang, Y. Xiao, S.H. Liu, Y. Li, Q.Y. Cai, S.L. Luo, G.M. Zeng, Appl. Catal. B: Environ. 94 (2010) 142.
[6] K.L. Lv, X.F. Li, K.J. Deng, J. Sun, X.H. Li, M. Li, Appl. Catal. B: Environ. 95 (2010) 383.
[7] J. Moon, C. Yun, K. Chung, M. Kang, J. Yi, Catal. Today 87 (2003) 77.
[8] Y. Cho, H. Kyung, W. Choi, Appl. Catal. B: Environ. 52 (2004) 23.
[9] S. Kaur, V. Singh, Ultrason. Sonochem. 14 (2007) 531.
[10] S. Liu, X. Chen, J. Hazard. Mater. 152 (2008) 48.
[11] F. Chen, W. Zou, W. Qu, J. Zhang, Catal. Commun. 10 (2009) 1510.
[12] A. Jirapat, K. Puangrat, S. Supapan, J. Hazard. Mater. 168 (2009) 253.
[13] R. Asahi, T. Morikawa, T. Ohwaki, K. Aoki, Y. Tage, Science 293 (2001) 269.
[14] C. Chang, J. Xu, L. Jiang, D. Mao, W. Ying, Mater. Chem. Phys. 98 (2006) 509.
[15] C. Zhao, D. Chen, Mater. Lett. 61 (2007) 3673.
[16] S. Yin, Y. Aita, M. Komatsu, J. Wang, Q. Tang, T. Sato, J. Mater. Chem. 15 (2005) 674.
[17] S. Yin, H. Hasegawa, D. Maeda, M. Ishitsuka, T. Sato, J. Photochem. Photobiol. A: Chem. 163 (2004) 1.
[18] H.H. Li, S. Yin, T. Sato, Nanoscale Res. Lett. 6 (2011) 5.
[19] S. Yin, B. Liu, P.L. Zhang, T. Morikawa, K. Yamanaka, T. Sato, J. Phys. Chem. C 112 (2008) 12425.
[20] S. Yin, P.L. Zhang, B. Liu, X.W. Liu, T. Sato, D. Xue, S. Lee, Res. Chem. Intermed. 36 (2010) 69.
[21] Y. Lin, Z. Tang, Z. Zhang, C. Nan, J. Eur. Ceram. Soc. 23 (2003) 175.
[22] X. Teng, W. Zhuang, Y. Hu, C. Zhao, H. He, X. Huang, J. Alloys Compd. 458 (2008) 446.
[23] T. Katsumata, T. Nabae, K. Sasajima, S. Komuro, T. Morikawa, J. Electrochem. Soc. 144 (1997) 243.
[24] H.H. Li, S. Yin, T. Sato, Appl. Catal. B 106 (2011) 586.